

# High-Resolution Imaging Using Integrated Optical Systems

S. Prasad,<sup>1</sup> T. C. Torgersen,<sup>2</sup> V. P. Pauca,<sup>2</sup> R. J. Plemmons,<sup>3</sup> J. van der Gracht<sup>4</sup>

<sup>1</sup> Center for Advanced Studies, University of New Mexico, Albuquerque, NM 87131

<sup>2</sup> Department of Computer Science, Wake Forest University, Winston-Salem, NC 27109

<sup>3</sup> Departments of Computer Science and Mathematics, Wake Forest University, Winston-Salem, NC 27019

<sup>4</sup> Holospex, Inc., 6470 Freetown Rd., Suite 200-104, Columbia, MD 21044

Received 15 February 2004; accepted 31 March 2004

**ABSTRACT:** Certain optical aberrations, such as defocus, can significantly degrade the signal collected by an imaging system, producing images with low resolution. In images with depth-dependent detail, such degradations are difficult to remove due to their inherent spatially varying nature. In 1995, Dowski and Cathey introduced the concept of wavefront coding to extend the depth of field. They showed that wavefront coding and decoding enables quality control of such images using integrated optical-digital imaging systems. With wavefront coding, a high-resolution image can be efficiently obtained without the need to resort to expensive algorithms for spatially varying restoration. In this article, we discuss a novel and effective multiple-design-parameter approach for optimizing the processes of encoding and decoding the wavefront phase in integrated optical-digital imaging systems. Our approach involves the use of information metrics, such as the Strehl ratio and Fisher information, for determining the optimal pupil-phase distribution for which the resulting image is insensitive to certain aberrations, such as focus errors. The effectiveness of this approach is illustrated with a number of numerical simulation experiments, and applications to the development of iris recognition systems with high-resolution capabilities are briefly discussed. © 2004 Wiley Periodicals, Inc. *Int J Imaging Syst Technol*, 14, 67–74, 2004; Published online in Wiley InterScience (www.interscience.wiley.com). DOI 10.1002/ima.20009

**Key words:** integrated imaging; wavefront coding; pupil-phase engineering; Fisher information; Strehl ratio; focus extension; nonlinear optimization; image restoration

## I. INTRODUCTION

Conventional optical imaging systems are constrained by a fundamental tradeoff between depth of field and light gathering. Large numerical aperture systems provide efficient use of the available light, but result in blurred imagery away from the plane of best focus. Stopping down the aperture increases the depth of field, but can result in low contrast and noise-dominated images because of decrease in optical flux reaching the image plane. Furthermore, a

decrease in aperture size worsens the diffraction limited resolution at the in-focus plane. The laboratory images in Figure 1 illustrate this trade-off between the depth of field and the optical flux.

In an electronic imaging system, post-detection image restoration may be used to address the problem of limited depth of field. The image of a complicated 3D scene collected by a wide-aperture imaging system will contain regions corresponding to many different object distances that are each blurred by a unique defocused point spread function (PSF). A general approach to restoring such an image will involve spatially variant blind deconvolution. Blind deconvolution is a difficult computational problem that requires *a priori* information about the nature of the scene. Furthermore, image regions corresponding to large amounts of defocus will typically result in very low modulation transfer function (MTF) values for mid to high spatial frequencies, which often causes in unstable image restorations (Engl et al., 1996).

In a seminal article Dowski and Cathey (1995) proposed, an imaging modality known as *wavefront coding*, which involves the use of a cubic phase mask, of the form

$$\phi(x, y) = a(x^3 + y^3), \quad (1)$$

in the pupil of a standard limited-focus imaging system to encode a 3D scene so as to produce an intermediate image with a nearly spatially invariant blur corresponding to a known point spread function (PSF). The  $x$  and  $y$  coordinates are in the pupil plane. The multiplier  $a$  determines the strength of the phase mask. Signal processing is then employed to digitally restore the intermediate image (see Figure 2). Under suitable conditions, such restored images exhibit excellent depth-dependent detail. Without any phase encoding such detail would be washed out due to normal focus-dependent blur. In recent years, wavefront coding has been extended to include more general cubic-type surfaces or masks by Cathey, Dowski, and others at CDM-Optics, Inc., Boulder, CO (Bradburn et al., 1997; Cathey and Dowski, 2002; Dowski et al., 2000; Kubala et al., 2003). These integrated focus-invariant imaging systems can have more than an order of magnitude increase in depth of field

Correspondence to: R. J. Plemmons; e-mail: plemmons@wfu.edu

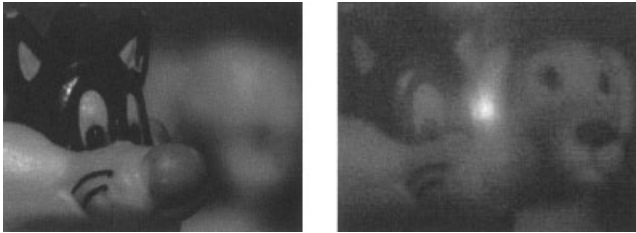


**Figure 1.** Low-resolution images resulting from a limited depth of field (left) and from stopping down the aperture to increase the depth of field (right).

(Cathey and Dowski, 2002). Figure 3 shows a scene photographed without the use of a cubic phase mask (left), the same subject photographed with a cubic phase mask (center), and the corresponding restored image (right).

We have recently introduced a new paradigm, called *pupil-phase engineering* (PPE), to optimize the design of more general pupil-phase masks that may lead to even better performance than the standard cubic mask in extending the depth of focus (Prasad et al., 2002, 2003). Two PPE approaches were proposed, one using Strehl ratio (SR) and the other using Fisher information (FI) as metrics of performance of such integrated optical-digital imaging systems. The SR is proportional to the on-axis value of the PSF as a function of defocus. Candidate designs are pupil-phase masks that make the first few derivatives of the SR with respect to the defocus parameter small without degrading the SR greatly. The FI metric uses the full PSF, not just its on-axis values, and measures the sensitivity of the PSF to defocus. Candidate designs lead to pupil-phase masks that minimize the FI metric, i.e., minimize the sensitivity of the PSF to defocus, while keeping the SR sufficiently high.

In the present article, we elaborate further on both optimization approaches. As noted, the latter approach uses the full PSF, not just its on-axis value that defines the SR, and is based formally on the concept of Fisher information (FI) used in statistical estimation theory (Dowski, 1995; Van Trees, 1968). The FI furnishes a particularly simple measure of focus independence, as we shall see. It also has the merit of having been studied extensively over the past several decades, and its rich theoretical framework may enable a deeper understanding of the general subject of pupil-phase encoding. The use of FI in the context of imaging is not new. It has been previously discussed in the context of estimation of a variety of object parameters from noisy image data, including the estimation of the object when its range is unknown (Dowski, 1995). Also, Dowski and Cathey (1995) used FI to evaluate the behavior of cubic phase masks in the spatial-frequency domain. Here, we use FI in the physical domain to furnish an optimization criterion for deducing the best phase mask under a range of imaging conditions.

The present work is limited to the use of PPE to treat the problem of focus extension. The PPE concept is more general, however, and may also be employed for a number of other useful applications that

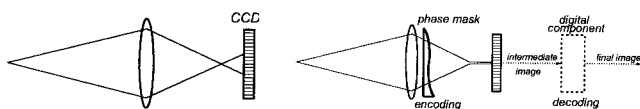


**Figure 2.** Diagrams of conventional (left) and integrated optical-digital (right) systems.



**Figure 3.** Application of the cubic phase mask.

range from static aberration control to a reduction of focal depth (Sherif and Cathey, 2001).

We begin this paper in Section II by discussing a number of classes of pupil phase masks that can be employed to remove the defocus blur in a well corrected imaging system. In Section III, we present our two main PPE approaches, based on the SR and FI metrics, and discuss their implementation. The results of numerical optimization within each of the various classes of phase masks are presented in Section IV. In Section V, we compare our optimized phase masks with one another and with pure cubic phase masks by using the SR and MTF as metrics of performance. Our simulated 3D cone-shaped object is described in Section VI. We present in Section VII the results of our numerical simulations of pupil-phase encoded images of our simulated object at different focal depths, which are deblurred digitally with a single in-focus PSF. The relatively high resolution of the restored images clearly demonstrates the effectiveness of our PPE approach in removing the defocus blurs. Some summary remarks are provided in Section VIII, including a brief discussion of applications of our current work with CDM-Optics Inc., to the development of iris recognition systems with high-resolution imaging capabilities important for personnel identification and verification.

## II. PUPIL PHASE MASKS

A number of phase profiles can be employed in the pupil to encode images of objects possessing a finite depth coordinate. The original proposal (Dowski and Cathey, 1995) argued for a cubic phase mask based on the requirement that the phase  $\phi(x, y)$  be monomial in the pupil coordinates  $(x, y)$ , separable in those coordinates, and lead to an MTF that is asymptotically focus-independent. Those results have also been extended by researchers at CDM-Optics to more general surfaces or masks (Bradburn et al., 1997; Cathey and Dowski, 2002; Dowski et al., 2000; Kubala et al., 2003), by using techniques such as ray tracing. By contrast, our PPE approach calls for a pupil function based on requirements we place in the physical domain, namely, those based on the PSF. In view of the generality of our approach, we discuss a number of classes of phase functions within which we can optimize the encoding pupil phase.

The most general power-series form of the phase  $\phi(x, y)$  is the following:

$$\phi(x, y) = \sum_{m=0}^{\infty} \sum_{n=0}^{\infty} a_{mn} x^m y^n. \quad (2)$$

We henceforth exclude the constant ( $a_{00}$ ) and linear ( $a_{10}, a_{01}$ ) terms, which represent piston and tip-tilt phases that are of no consequence here. Symmetry arguments can help constrain the form of the phase function further. If we require that the phase function be optimized equally relative to the  $x$  and  $y$  coordinate axes, then it must be

invariant under an  $x \leftrightarrow y$  exchange operation. Excluding the constant and linear terms, we then have the following form for  $\phi$ :

$$\phi(x, y) = axy + b(x^2 + y^2) + c(x^3 + y^3) + d(x^2y + xy^2) + \dots \quad (3)$$

where the ellipses represent fourth- and higher-order terms. It is easy to see that there are at most  $(\lfloor n/2 \rfloor + 1)$  coefficients in the  $n$ -th order, where  $\lfloor z \rfloor$  is the largest integer smaller than or equal to  $z$ .

Further constraints on the phase can be placed by requiring that it be odd under coordinate inversion,  $\phi(-x, -y) = -\phi(x, y)$ . Such phase forms, as we showed previously (Prasad et al., 2003), lead to Strehl ratios and PSFs that are both even in the defocus parameter. This evenness implies that the Taylor expansions of these quantities only contain even powers of defocus. This is desirable because all odd powers are automatically absent and thus do not require any optimization considerations.

Another useful regrouping of terms in expansion (3) that is suggestive of various optical aberrations is furnished by the Zernike polynomials. The different low-order Zernikes we use in our defocus problem, along with their names, are listed below.

$Z_4(r, \theta) = \sqrt{3}(2r^2 - 1)$	defocus
$Z_5(r, \theta) = \sqrt{6}r^2 \sin 2\theta$	astigmatism, 45°
$Z_6(r, \theta) = \sqrt{6}r^2 \cos 2\theta$	astigmatism, 0°
$Z_7(r, \theta) = \sqrt{8}(3r^3 - 2r)\sin \theta$	coma, x-direction
$Z_8(r, \theta) = \sqrt{8}(3r^3 - 2r)\cos \theta$	coma, y-direction
$Z_9(r, \theta) = \sqrt{8}r^3 \sin 3\theta$	field curvature, 30°
$Z_{10}(r, \theta) = \sqrt{8}r^3 \cos 3\theta$	field curvature, 0°

where the polar coordinates  $(r, \theta)$  are simply related to the Cartesian coordinates used so far,  $x = r \cos \theta$ ,  $y = r \sin \theta$ . We employ a truncated version of expansion (2) that uses only low-order Zernike polynomials. Because terms linear in  $x, y$  occur in a number of these polynomials, we normally subtract out such terms from our expansion before optimizing it. We now present a more detailed theoretical background underlying our pupil-phase engineering approach.

### III. OPTIMIZING THE PUPIL PHASE: THEORY

We adopt two different strategies to determine the actual coefficients in the various forms of the pupil phase we have just discussed. They are both based on considerations of the PSF  $h(r; \tau)$  in the image plane [coordinate vector:  $\mathbf{r} = (s, t)$ ],

$$h(\mathbf{r}; \tau) = |K(\mathbf{r}; \tau)|^2, \quad (4)$$

where  $K$  is the following pupil integral:

$$K(\mathbf{r}; \tau) = \frac{1}{\lambda f \sqrt{A}} \iint P(\boldsymbol{\rho}) e^{i[(2\pi/\lambda f)r \cdot \boldsymbol{\rho} + \phi(\boldsymbol{\rho}) + \tau \rho^2]} dx dy. \quad (5)$$

In this expression,  $\boldsymbol{\rho} = (x, y)$ , where  $x$  and  $y$  are coordinates in the pupil plane, and  $\rho = \sqrt{x^2 + y^2}$ . Also,  $P(\boldsymbol{\rho})$  is the pupil function, equal to 1 inside the pupil and 0 outside for a clear pupil,  $\phi(\boldsymbol{\rho})$  is the pupil phase above and beyond the defocus phase  $\tau \rho^2$ ,  $\mathbf{r} \cdot \boldsymbol{\rho}$  denotes the dot product of vectors  $\mathbf{r}$  and  $\boldsymbol{\rho}$ ,  $\lambda$  is the wavelength of illuminating light,  $f$  is the focal length, and  $A$  is the area of the pupil. The use of vector

notation lends brevity to the formulas, as they will be used again in the article.

**A. Strehl-Ratio-Based Optimization.** The Strehl ratio (SR) is the ratio of the on-axis values of the PSF with and without the pupil phase. For phase masks that are odd under parity (or coordinate inversion,  $x \rightarrow -x, y \rightarrow -y$ , i.e.,  $\boldsymbol{\rho} \rightarrow -\boldsymbol{\rho}$ ),

$$\phi(-\boldsymbol{\rho}) = -\phi(\boldsymbol{\rho}), \quad (6)$$

the following expression for the SR may be derived:

$$\chi(\tau) = \frac{1}{A^2} \iiint P(\boldsymbol{\rho}) P(\boldsymbol{\sigma}) \cos \phi(\boldsymbol{\rho}) \cos \phi(\boldsymbol{\sigma}) \times \cos[\tau(\rho^2 - \sigma^2)] dx dy du dv, \quad (7)$$

where  $\sigma \sqrt{u^2 + v^2}$ , with  $(u, v)$  being a point in the pupil plane. The  $\tau$ -dependent cosine term may now be expanded in its Taylor series to yield the following even-power series for the SR:

$$\chi(\tau) = \sum_{n=0}^{\infty} \chi_{2n} \tau^{2n}, \quad (8)$$

where the coefficients  $\chi_{2n}$  have the value

$$\chi_{2n} = \frac{(-1)^n}{n!} \frac{1}{A^2} \iiint P(\boldsymbol{\rho}) P(\boldsymbol{\sigma}) \cos \phi(\boldsymbol{\rho}) \cos \phi(\boldsymbol{\sigma}) \times (\rho^2 - \sigma^2)^{2n} dx dy du dv. \quad (9)$$

A use of the binomial expansion

$$(\rho^2 - \sigma^2)^{2n} = \sum_{m=0}^{2n} (-1)^m \binom{2n}{m} \rho^{2m} \sigma^{4n-2m} \quad (10)$$

then reduces the double-pupil-integral form (9) to one involving only *single* pupil integrals,

$$\chi_{2n} = \frac{(-1)^n}{n!} \sum_{m=0}^{2n} (-1)^m \binom{2n}{m} C_{2m} C_{4n-2m}, \quad (11)$$

where

$$C_\ell = \frac{1}{A} \iint P(\boldsymbol{\rho}) \rho^\ell \cos[\phi(\boldsymbol{\rho})] dx dy \equiv \langle \rho^\ell \cos[\phi(\boldsymbol{\rho})] \rangle, \quad (12)$$

the triangular brackets indicating an average of the quantity they enclose over the pupil function.

Our optimization procedure is based on making the terms labeled by  $n = 1, \dots, (N - 1)$  in expansion (8) small, for some chosen  $N$ , so that the first significant  $\tau$ -dependent term of that expansion is  $O(\tau^{2N})$ , subject to “regularization” constraints on the magnitude of the SR at  $\tau = 0$ , namely on  $\chi_0$ , and the parameters of the pupil phase  $\phi(\boldsymbol{\rho})$ . We implement this procedure by seeking to minimize the

squared norm of the vector  $(\chi_2, \dots, \chi_{2N-2})$  to which are added appropriate regularization terms.

For pupil phases that are not odd under any of the symmetries (coordinate inversion being one such) of the pupil function  $P(\boldsymbol{\rho})$ , odd powers in  $\tau$  also occur in the expansion, and the expression for the coefficients  $\chi_n$  is also more involved (Prasad et al., 2002) than Eq. (11). The preceding optimization procedure must be accordingly modified.

**B. FI-Based Optimization.** The Fisher information (FI) metric we propose uses the full PSF, rather than just its on-axis value that defines the SR. Any odd-parity phase mask gives rise to a PSF that, like the SR, has the desirable property of containing no odd powers of the defocus parameter  $\tau$ . The following expression for the PSF explicitly demonstrates this fact:

$$h(\mathbf{r}; \tau) = \frac{1}{A^2} \iiint P(\boldsymbol{\rho})P(\boldsymbol{\sigma}) \cos \left[ \frac{2\pi}{\lambda f} \mathbf{r} \cdot (\boldsymbol{\rho} - \boldsymbol{\sigma}) + \phi(\boldsymbol{\rho}) - \phi(\boldsymbol{\sigma}) \right] \times \cos[\tau(\rho^2 - \sigma^2)] dx dy du dv.$$

The FI that measures the sensitivity of the PSF to defocus may be defined (Van Trees, 1968) as the following image-plane integral:

$$J(\tau) = \iint h(\mathbf{r}; \tau) \left[ \frac{\partial \ln h(\mathbf{r}; \tau)}{\partial \tau} \right]^2 ds dt = \iint \frac{1}{h(\mathbf{r}; \tau)} \left[ \frac{\partial h(\mathbf{r}; \tau)}{\partial \tau} \right]^2 ds dt. \quad (13)$$

Instead of the squared norm of the vector of coefficients of the SR, we can seek to minimize the sum of  $J(\tau = 0)$  and the usual regularizing terms. The problem with such a simple approach is that  $J(\tau)$  vanishes identically for zero defocus,  $\tau = 0$ , for any odd-parity phase mask, because the PSF has no  $O(\tau)$  terms in its Taylor expansion. We could define  $J$  in such situations to be relative to the squared-defocus parameter,  $\tau_2 \equiv \tau^2$ , not  $\tau$ , noting that  $J(\tau_2)$  does not vanish at  $\tau = 0$ , in general, for *any* phase mask. Alternatively, we could use, instead of  $J(0)$ , the following integral of  $J(\tau)$ :

$$I(\tau_0) = \int_{-\tau_0}^{\tau_0} J(\tau) d\tau, \quad (14)$$

where  $(-\tau_0, \tau_0)$  denotes the (symmetric) range of defocus parameters of interest for the physical problem at hand. In this article, we use only the metric (14) for all FI-based optimizations of the pupil phase mask.

In both SR-based and FI-based approaches, additive regularization terms are essential to constrain the choice of the optimal phase mask from reaching the trivial, physically uninteresting solution of an infinitely large phase and an identically vanishing PSF. We therefore constrain our optimization procedure by requiring that the resulting SR not fall below a minimum threshold value, determined essentially by how robust the restoration algorithm is against falling SR values in the presence of noise. The following Fermi–Dirac regularization term implements this requirement:

$$J_\chi(\mathbf{u}) = M[1 - \chi(0, \mathbf{u})] \frac{1}{e^{k[\chi(0, \mathbf{u}) - \bar{\chi}]} + 1}, \quad (15)$$

where  $\chi(0, \mathbf{u})$  is the Strehl ratio at zero defocus,  $\mathbf{u}$  is the vector of phase-mask coefficients being sought,  $M$  is a positive constant representing the maximum penalty,  $k$  is a large positive constant that determines the steepness of the “cutoff edge,” and  $\bar{\chi}$  represents the minimum acceptable SR. For small SNR, both  $k$  and  $\bar{\chi}$  are expected to scale inversely with SNR.

A numerically improved form of the FI metric (13) is possible in which the divergence of the integrand at positions  $\mathbf{r}$  where the PSF vanishes is explicitly removed. This form for  $J$  involves the complex amplitude  $K(\mathbf{r}; \tau)$  whose squared modulus is the PSF. In terms of  $K$  and  $K^*$ , given by Eq. (5) and its complex conjugate, expression (13) for  $J(\tau)$  may be cast in the form

$$J(\tau) = \iint \frac{1}{KK^*} \left( K \frac{\partial K^*}{\partial \tau} + K^* \frac{\partial K}{\partial \tau} \right)^2 ds dt = \iint \left[ \frac{K}{K^*} \left( \frac{\partial K^*}{\partial \tau} \right)^2 + \frac{K^*}{K} \left( \frac{\partial K}{\partial \tau} \right)^2 + 2 \frac{\partial K}{\partial \tau} \frac{\partial K^*}{\partial \tau} \right] ds dt. \quad (16)$$

Note that the ratio  $K/K^*$  is unimodular and finite, being equal to  $\exp[2i \arg(K)]$ .

#### IV. OPTIMIZATION OF THE PUPIL PHASE: NUMERICAL RESULTS

A number of classes of masks have been considered in our work. We present details of optimization for symmetric mixed cubic masks of form (3) with  $a = b = 0$ , although results corresponding to optimized Zernike masks discussed earlier in Section II and also in an earlier article (Prasad et al., 2002), will also be used for comparison.

**A. SR-Based Optimization Results.** Because the symmetric mixed mask of degree 3 has two independent coefficients  $c$  and  $d$ , one can in general hope for at most two of the SR derivatives,  $\chi_{2n}$ , to be made as small as we please. Because in general there are a whole infinite set of solution pairs  $(c, d)$  possible and both the sensitivity of the SR to defocus and the SR decrease with increasing  $|c|, |d|$ , only one or at most a few of these solutions pairs will be optimal in the sense of meeting the requirement of maximum possible insensitivity to defocus consistent with the constraint of a minimum SR threshold. The purpose of the nonlinear optimizer is to find these optimal solutions approximately by minimizing the objective function

$$J_{\text{SR}}(c, d) = [\chi_2(c, d)]^2 + [\chi_4(c, d)]^2 + M[1 - \chi_0(c, d)] \frac{1}{e^{k[\chi_0(c, d) - \bar{\chi}]} + 1}. \quad (17)$$

An additional penalty term of form  $\gamma[c^2 + d^2]$  can be added to prevent the coefficients from becoming too large. However, we usually ignore such a term in our calculations.

The objective function is highly oscillatory with numerous local minima in the  $(c, d)$  plane. A Monte-Carlo-type technique is therefore used for the global optimization. Uniformly random starting points were chosen in a closed region  $\mathcal{R} = [-50, 50] \times [-50, 50]$ , and the Levenberg–Marquart method was applied to find a corresponding local minimum of the objective function (17) for each

starting point. A total of 500 starting points were chosen. The set of solutions were sorted according to the Strehl-based metric, excluding the penalty term. The solution with the lowest value for the Strehl metric (most insensitivity to defocus) that lies on or near the boundary implied by the penalty term (greatest strength possible satisfying the Strehl constraint) was selected.

The optimal-solution found for the symmetric basis of total degree three is given by

$$(c, d) = (36.5961, -50.3604),$$

i.e., the pupil phase mask is given by the function:

$$\phi(x, y) = 36.5961(x^3 + y^3) - 50.3604(x^2y + xy^2). \quad (18)$$

The minimum value of the objective function corresponding to the coefficients in Eq. (18) is the squared Euclidean norm of the following vector:

$$\mathbf{fvec} = [1.04659e - 08, 5.82893e - 08, 2.33977e - 06].$$

The components of the vector  $\mathbf{fvec}$  are  $\chi_2$ ,  $\chi_4$ , and  $J_\chi(c, d)$ , respectively.

The values of  $\chi_2$  and  $\chi_4$ , proportional to the second and fourth derivatives of SR with respect to defocus, are *very* small. Thus, we should expect very good insensitivity to defocus in this example, and the simulation tests support this, as we shall see later. For this phase mask, we can also see some geometric distortion. This should not cause any surprise or disappointment, since the SR-based metric really cannot control distortion with respect to defocus. The full PSF in this example resembles the PSF of phase masks we have seen in previous work using the Zernike basis as well. However, the expediency of a low-dimensional parameter search characteristic of the symmetric phase masks, as well as its overall simplicity, make it a superior choice to the Zernike phase mask.

**B. FI-Based Optimization Results.** A similar MonteCarlo approach of starting the Levenberg–Marquardt method of minimization with uniformly random starting points in the closed region  $\mathcal{R} = [-50, 50] \times [-50, 50]$  of the  $(c, d)$  plane was applied in this case as well. The objective function  $J(c, d)$  is different, however, and given by the expression

$$J(c, d) = \sum_{\tau \in S} [J_f(\tau)]^2 + J_\chi(c, d), \quad (19)$$

where  $J_f(\tau)$  is the FI discussed earlier,  $S$  is a set of defocus ( $\tau$ ) values of interest, and  $J_\chi(c, d)$  is the penalty function used previously to enforce a minimum SR. The set  $S$  of values of  $\tau$  is chosen to be

$$S = \{1, 3, 5, 7, 9, 11, 13, 15, 17, 19\}. \quad (20)$$

The sum in Eq. (19) approximates the integral of  $[J_f(\tau)]^2$  over the range  $(0, 19)$  in  $\tau$ , or equivalently half of that integral over the range  $(-19, 19)$  since  $J_f(\tau)$  is even in  $\tau$  for the symmetric phase mask.

A total of 40 uniform random starting points were chosen, and the solutions were sorted according to the FI-based metric in Eq. (19), excluding the penalty term. The solution with the lowest value for the FI metric (most insensitivity to defocus) that lies on or near the boundary implied by the penalty term (greatest strength possible

satisfying the Strehl constraint) was selected. The optimal solution found for the symmetric basis of total degree 3 is given by:

$$a = [32.6809, -102.027],$$

i.e., the pupil phase mask is given by the function:

$$\phi(x, y) = 32.6809(x^3 + y^3) - 102.027(x^2y + xy^2). \quad (21)$$

The minimum value of the objective function corresponding to the coefficients in Eq. (21) is the squared Euclidean norm of the following vector:

$$\mathbf{fvec} = [0.00105885, 0.00363798, 0.00569221, 0.00899365, \\ 0.0127826, 0.0166305, 0.02045, 0.0241882, \\ 0.0275795, 0.0307985, 0.00837011].$$

The first 10 components of  $\mathbf{fvec}$  correspond to the FI metric function  $J_f(\tau)$  for the values of  $\tau \in S$  defined in (20). The last component of  $\mathbf{fvec}$  corresponds to the  $J_\chi(c, d)$  penalty term in Eq. (19). The values of  $J_f(\tau)$  are small, so we can hope for good insensitivity to defocus.

## V. SR-BASED AND MTF-BASED COMPARISONS OF VARIOUS OPTIMIZED PHASE MASKS

Before addressing the relative performance of the various phase masks in the imaging of a simulated 3D object, we evaluate them in terms of two elementary metrics of image quality, namely their SR and MTF values. For this comparison, we choose the two symmetric mixed cubic phase masks optimized according to our SR- and FI-based metrics of the previous section as well as the SR-optimized Zernike phase mask (Prasad et al., 2002) and the pure cubic mask (Dowski and Cathey, 1995). The two symmetric mixed cubic masks refer to the mask given by Eq. (3) with  $a = b = 0$ . The values of  $c$  and  $d$  are 32.6809 and  $-102.027$  for the FI-optimized mask and 36.5961 and  $-50.3604$  for the SR-optimized mask. For the chosen Zernike mask, the only non-vanishing coefficients of the Zernike polynomials in the phase mask are those for  $Z_5, \dots, Z_{10}$ ; they were determined (Prasad et al., 2002) to be  $-0.007581, 0.1349, -3.707, 3.512, 0.5899, 0.7914$ , respectively. For the pure cubic mask, three different strengths were chosen for which the same in-focus SR values as for the optimized symmetric mixed cubic and Zernike masks are obtained. These cubic mask strengths were found to be close to 9.8, 20, and 40.

In Figure 4, we plot the SR as a function of the defocus parameter  $\tau$  for the various masks described above. Note the essentially flat SR versus defocus curves for both the FI optimized and Zernike cases, reflecting excellent optimization. The pure cubic mask does not exhibit good focus independence for small to moderate defocus values, except for the highest-strength case.

A somewhat different comparison uses the MTF as a metric of both focus invariance and of image restorability. We concentrate here on the image restorability alone, by plotting the discretized form of the angularly averaged in-focus MTF, namely,

$$M(\nu) = \frac{1}{2\pi} \int_0^{2\pi} |H(\nu, \theta)| d\theta, \quad (22)$$

where  $H(\nu, \theta)$  is the in-focus OTF expressed in polar coordinates in which  $\nu$  is the magnitude of the spatial frequency and  $\theta$  is the

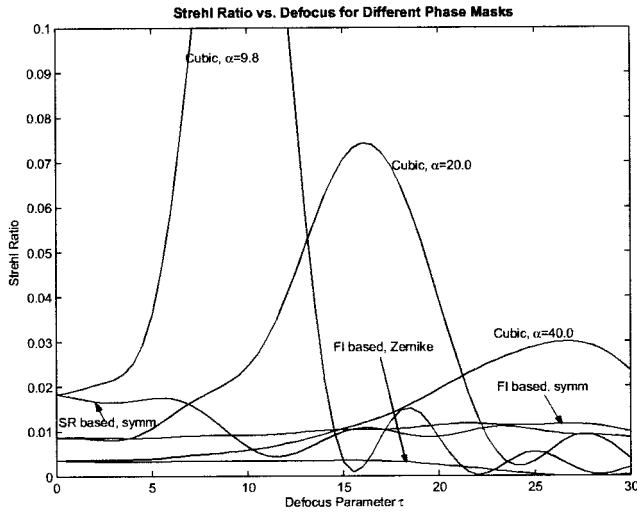


**Figure 4.** Strehl ratio versus defocus for a number of phase masks. The phase masks and the values of their coefficient parameters are specified in the text.

azimuthal angle of the spatial-frequency vector. In Figure 5, we display this average as a function of  $\nu$  for the same six masks that were used in the previous figure. In all cases, this mean MTF seems to be well off the zero floor at nearly all frequencies that are not too close to the cut-off, but the pure cubic phase masks have generally the highest MTF in the mid-frequency range in all cases. Notwithstanding this observation, we may not use it to make any robust judgments about which phase mask will lead to better restorability of 3D objects. That is so for two reasons. First, what is needed for good restoration is that the MTF values simply be well above the noise floor over the frequencies of interest. A study of the noise floor that separates a certain signal space of larger MTF values from a certain noise space of smaller MTF values is currently under way. Second, the MTF is only half the story. What is of importance is also the phase of the OTF, which together with MTF determines the full PSF, and it is the focus invariance of the full PSF, or equivalently of

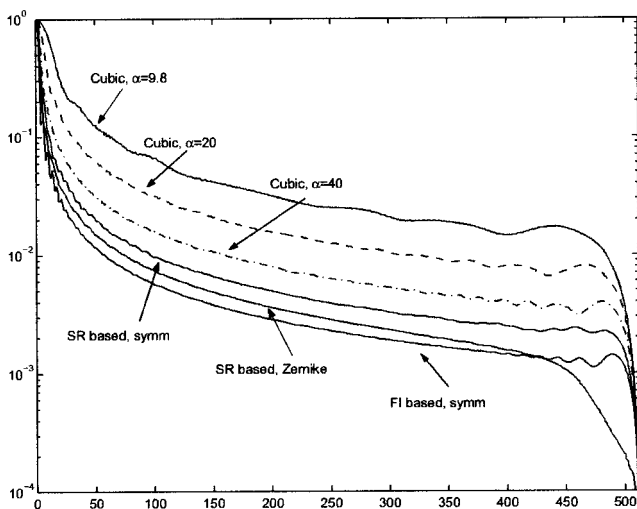


**Figure 5.** Angularly averaged in-focus MTF as a function of spatial frequency (in pixel units), for the six masks of the previous figure.

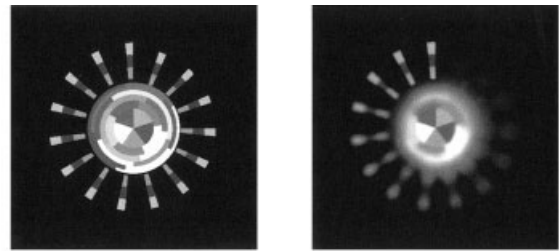


**Figure 6.** Simulated parabolic cone-shaped object.

the full OTF, that is of greater relevance to the focus extension problem. Pure cubics, although ensuring good focus invariance of the MTF, do suffer from the problem of having a significant depth-dependent phase for their OTF.

Our FI-optimized phase masks work with the full PSF and furthermore take both the defocus range and overall SNR value into consideration. They are thus likely to provide the highest depth of focus in the phase-encoded image. The correspondingly excellent focus invariance of the PSF should then lead to restorations that should resolve the depth detail well. This expectation is verified in Section VII where we simulate a 3D object, image it with different optical systems containing the different pupil phase masks we have discussed here, and then restore the optical images.

## VI. COMPUTER MODELING AND OPTICAL SYSTEM SIMULATION

Numerically computed phase mask designs are tested using a computer simulation software system developed by the authors. The simulator models a parabolic cone-shaped object surrounded by a set of wings arranged in a spiral at equal angles and linearly progressive distances away from a reference plane coincident with the center point. The central point is thus visually nearest the observer, while the wings spiral away in the counter-clockwise direction. Each point in the object is blurred by a spatially varying PSF that models the appropriate defocus according to the distance from that point to the reference plane. For improved performance, the modeled object is decomposed into point sets equidistant from the reference plane (and thus equally blurred). The usual Fourier-transform-based convolution methods are applied to each point set. The simulated scattered light energy from each point set is then summed together to produce the final simulated image.

Figure 6 illustrates the effect of noise-free spatially varying defocus. For comparison, a theoretical blur-free perspective projection of the object is also shown on the left. The authors' software simulates the effect of a pupil-phase encoding phase mask by adding

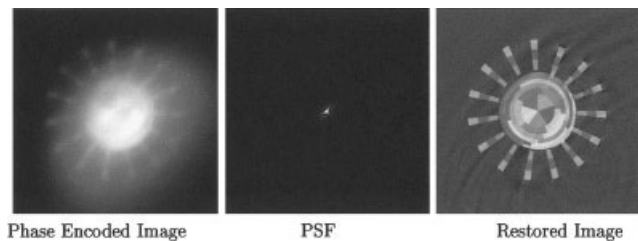


**Figure 7.** The phase-encoded blurred image, the PSF, and the restored image for the SR-optimized phase mask described in the text.

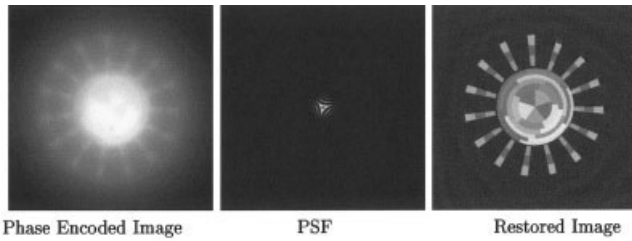


**Figure 8.** The phase-encoded blurred image, the PSF, and the restored image for the FI-optimized phase mask described in the text.

a chosen fixed pupil-phase function to the defocus (quadratic) phase as each point set is processed.

## VII. PUPIL PHASE ENCODING AND IMAGE RESTORATION

The PPE optimization we have described in Sections III and IV makes no reference to the object being imaged. Rather it is based on a balancing of the focus insensitivity of the PSF with a minimum SR by nonlinear optimization techniques. We now describe how faithfully images of the simulated cone object encoded by these optimized phase masks can be restored by a simple Wiener filter under a given SNR estimate.

In Figures 7 and 8, we display the phase encoded image, the PSF of the encoding pupil phase mask of form (3), and the restored image. Additive Gaussian noise with an overall SNR of 100 was assumed in our simulations. The restoration uses a regularized Wiener filter with regularization parameter  $4e-06$ . Figure 7 employs the SR optimized symmetric mixed cubic mask with coefficients  $a = b = 0$ ,  $c = 36.5961$ ,  $d = -50.3604$ , and Figure 8 employs the corresponding FI-optimized mask with coefficients  $a = b = 0$ ,  $c = 32.6809$ ,  $d = -102.027$ . For comparison, we exhibit in Figure 9 the restorations with a pure cubic phase mask of strength 20 and 40, respectively. The pure cubic of strength 20 has the same in-focus SR as the FI-optimized mask, and the cubic of strength 40 was used here to see if and how much the performance improves by raising the cubic-mask strength. Note the visually superior restoration with the FI-optimized mask, for which not only is the SR most independent of defocus (see Fig. 4), but the PSF has a rather compact form with approximate triangular symmetry.

Visual impressions can often be deceptive, however. We therefore use a more objective criterion for ranking the restored images, that of taking the root mean squared error (RMSE) over the entire image. The RMSE per pixel,  $\Delta$ , is defined as follows:

$$\Delta^2 = \frac{1}{N^2} \sum_{m=1}^N \sum_{n=1}^N [\hat{f}(m, n) - f(m, n)]^2, \quad (23)$$

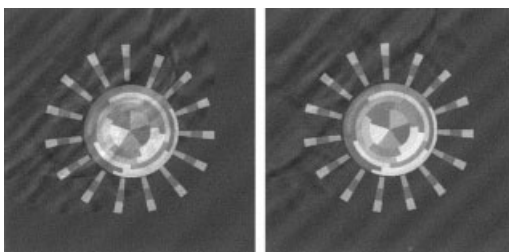


**Figure 9.** The restored images for a pure cubic phase mask, with cubic strength 20 (left) and 40 (right).

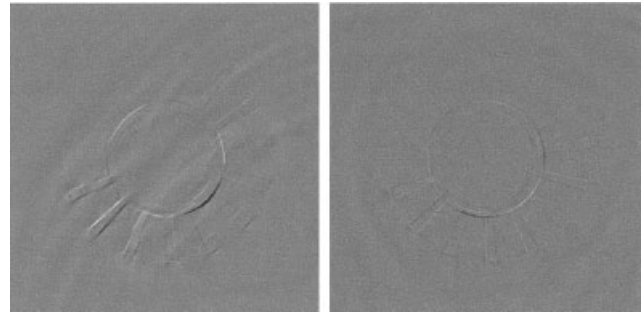


**Figure 10.** Simulated difference image (true object minus restored image) for the SR-optimized (left) and FI-optimized symmetric mixed cubic masks (right).

where the images are on an  $N \times N$  square pixel array, and  $\hat{f}(m, n)$  and  $f(m, n)$  are, respectively, the restored image and model object intensities at the pixel  $(m, n)$ .

We use the RMSE as a metric to compare the restorations of images encoded by our two optimized phase masks and by suitably chosen pure cubic phase masks. A preliminary choice of the strengths of the pure cubic mask is based on the simple requirement laid out in Section V namely, that the in-focus SR for the pure cubic be the same as the in-focus SR for the two PPE-optimized symmetric mixed cubic masks we have computed here. This single-parameter search was performed by computing the in-focus SR for a range of cubic strength values and inferring, by simple bisection interpolation, that strength value that has the correct SR.

In Figures 10 and 11, we display the difference images, each formed by subtracting the restored image from the true object, for the SR- and FI-optimized symmetric mixed cubic masks and two pure cubics of strength 20 and 40. The RMSE-per-pixel values in the Wiener restored images for the four masks in the order listed above are 0.0690, 0.0570, 0.0785, and 0.0658, respectively. Because the peak intensity value at a pixel in the model object was 0.906, these mean errors amount to 7.6%, 6.2%, 8.7%, and 7.3%, respectively, of that peak value. The FI-based symmetric mixed cubic mask thus outperforms the other three masks in this preliminary test, a fact that is also confirmed by the visual appearance of the various difference images. Raising the cubic strength does improve the restorations, but a fairer comparison of the performances of the symmetric mixed cubic and pure cubic phase masks would require applying the same exact optimization with which we compute the former to the latter phase masks. This work is in progress at present.

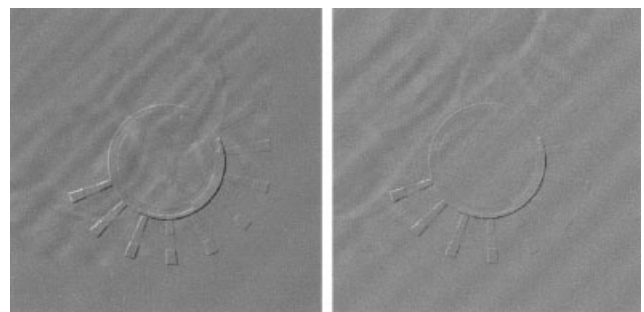


**Figure 11.** Simulated difference image (true object minus restored image) for a pure cubic mask of strength 20 (left) and of strength 40 (right).

To date, researchers have emphasized direct linear methods, such as the Wiener filter, to restore wavefront coded images (Bradburn et al., 1997; Dowski and Cathey, 1995) because of good computational efficiency that allows for real-time restoration. This has been the approach adopted here as well. In many applications, real-time results are essential and direct methods are used. In some applications, however, direct linear methods should be used only to identify regions of interest in real time, and more computationally intensive iterative algorithms could be subsequently applied in an attempt to improve restoration fidelity (Nagy et al., 1997). Van der Gracht et al. (2001) recently conducted a preliminary study of iterative restoration of wavefront-coded imagery for focus invariance. A more exhaustive study of this problem will appear in a future article.

## VIII. CONCLUSIONS AND CURRENT WORK

The present work generalizes our earlier investigations (Prasad et al., 2002) where we introduced the concept of pupil phase engineering, a mathematical approach to optimize the choice of pupil phase masks to improve the quality of digitally restored images. Two optimization metrics of particular interest to the problem of extending the depth of focus that we have considered here are the Strehl ratio and the Fisher information. Our basic approach is to seek good focus insensitivity of the PSF, subject to a minimum acceptable Strehl ratio needed for image restoration under given conditions of detection noise and over the range of defocus values of interest. Achieving the right balance between focus insensitivity and restorability requires solving nonlinear optimization problems in this approach.

Although the originally proposed cubic phase mask performs well under a wide range of conditions and has the advantage of simplicity, a more general polynomial mask can be better optimized to meet a more specific set of performance demands. The proposed PPE approach can, in fact, be regarded as providing a general framework in which to address a broad range of image improvement objectives, ranging from extension and reduction of the depth of focus to ameliorating any image degradations that arise from optical aberrations.

Assessing the relative effectiveness of the various phase masks in improving the quality of restored images under a variety of operating conditions and for different classes of objects will be a major focus of future work. We have also begun investigating several iterative restoration methods to deblur pupil-phase encoded imagery in order to explore more fully both the trade-off space of speed, accuracy, and robustness and the parameter space of SNR, defocus range, noise statistics, and mask parameters.

Although based only upon simulation studies, our numerical results reported here amply establish the validity of the pupil-phase engineering as a useful tool for improving image quality in integrated imaging systems. High-resolution imaging using integrated optical systems should have important applications in science and engineering, as we note next in the context of security systems based upon biometrics.

We conclude this article with some comments about our current work in conjunction with CDM-Optics to the development of biometric iris recognition systems with high-resolution imaging capabilities that are important for personnel identification and verification. A description of some of this work is given in the SIAM News article "Novel Imaging Systems Rely on Focus-Free Optics," in August 2003 (Mackenzie, 2003). Computational imaging systems can be used to advantage in iris recognition technology. A major difficulty in current iris recognition systems is a rather shallow depth of field that limits system usability and increases system complexity. In collaboration with CDM-Optics, we

are developing a computational imaging approach to iris recognition using Wavefront Coding. This approach greatly increases the depth of field over that possible with traditional optics while keeping sufficient recognition accuracy. In this approach, the combination of optics, detectors, and image processing all contribute to the iris recognition accuracy. We will describe different configurations of the optics and signal processing algorithms as well as results from these systems in papers being presented at SPIE conferences in 2004 (See, e.g., van der Gracht et al., 2004).

## ACKNOWLEDGMENTS

The authors gratefully acknowledge funding support from the Army Research Office under grant DAAD19-00-1-0540, and from the Air Force Office of Scientific Research under grants FA49620-01-1-0321, FA49620-02-1-0107, and FA49620-03-1-0215.

## REFERENCES

- S. Bradburn, E.R. Dowski, W.T. Cathey, 1997. Realizations of focus invariance in optical-digital systems with wavefront coding. *Appl Opt* 26:9157–9166.
- W.T. Cathey, and E.R. Dowski, 2002. New paradigm for imaging systems. *Appl Opt* 41(29):6080–6092.
- E.R. Dowski, 1995. An information theoretic approach to incoherent information processing systems. In *Signal Recovery and Synthesis*, Vol 11. OSA Technical Digest Series. Optical Society of America: Washington, DC, 1995, pp 106–108.
- E.R. Dowski, and W.T. Cathey, 1995. Extended depth of field through wavefront coding. *Appl Opt* 34:1859–1866.
- E.R. Dowski, and R.H. Cormack, Sarama SD. Wavefront coding: Jointly optimized optical and digital imaging systems. In Z. Rahman, R. Schowengerdt, S. Reichenbach, Ed. *Proc. SPIE Visual Information Processing IX*, 2000, vol. 4041, pp. 114–120.
- H. Engl, M. Hanke, and A. Neubauer, 1996. *Regularization of Inverse Problems*. Kluwer Academic: Dordrecht, The Netherlands, 1996.
- K. Kubala, E.R. Dowski ER, and W.T. Cathey, 2003. Reducing complexity in computational imaging systems. *Optics Express* 11(18):2102–2108.
- D. Mackenzie, 2003. Novel imaging systems rely on focus-free optics. *SIAM News*, 36(6):1,10.
- J.G. Nagy, V.P. Pauca, R.J. Plemmons, and T.C. Torgersen. 1997. Space-varying restoration of optical images. *J Opt Soc Amer A* 14(12):3162–3174.
- S. Prasad, T.C. Torgersen, V.P. Pauca, and R.J. Plemmons, 2002. Integrated optics systems for image quality control. In *Proc. 2002 AMOS Tech Conf*, Maui, HI, Sept 2002.
- S. Prasad, T.C. Torgersen, V.P. Pauca, R.J. Plemmons, and J. van der Gracht, 2003. Engineering the pupil phase to improve image quality. In Rahman Z, Schowengerdt R, Reichenbach S, Ed. *Proc. SPIE Visual Information Processing XII*, 2003, Vol. 5108, pp. 1–12.
- S. Sherif, and T. Cathey. 2001. A phase grating to reduce the depth of field of incoherent hybrid imaging systems. In *OSA Trends in Optics and Photonics (TOPS)*, Integrated Computational Imaging Systems. Optical Society of America: Washington, DC, 2001.
- H. Van Trees, 1968. *Detection, Estimation, and Modulation Theory*. Wiley: New York, 1968.
- J. van der Gracht, J.G. Nagy, V.P. Pauca, and R.J. Plemmons, 2001. Iterative restoration of wavefront coded imagery for focus invariance. In *OSA Trends in Optics and Photonics (TOPS)*, Integrated Computational Imaging Systems. Optical Society of America: Washington, DC, 2001.
- J. van der Gracht, V.P. Pauca, H. Setty, E.R. Dowski Jr, R.J. Plemmons, T.C. Torgersen, and S. Prasad, 2004. Iris recognition with enhanced depth-of-field image acquisition. In *SPIE Defense and Security Symposium*, Orlando, FL, 2004.